This paper is published inn Langmuir 36, 16, 4308—4316 (2020)
https://doi.org/10.1021/acs.langmuir.0c00288

Effect of a Cationic Surfactant on Droplet Wetting on Superhydrophobic Surfaces

Ahmed Aldhaleai and Peichun Amy Tsai*

Mechanical Engineering, University of Alberta, Edmonton, Alberta T6G 1H9, Canada

E-mail: peichun.amy.tsai@ualberta.ca

Abstract

We experimentally and theoretically examine the influence of a double chain cationic surfactant, didodecyldimethylammonium bromide (DDAB), on the wetting states and contact angles on superhydrophobic (SH) surfaces made of hydrophobic micro-cylinders. We use two types of micropatterns of different surface roughness, r, and packing fraction, ϕ, and vary nine dimensionless surfactant concentrations (C_S), normalized by the critical micelle concentration (CMC), in the experiments. At low C_S, some of the surfactant-laden droplets are in a gas-trapping, Cassie-Baxter (CB) state on the high-roughness microstructures. In contrast, some droplets are in a completely-wetting Wenzel (W) state on the low-roughness microtextures. We found that the contact angle of CB drops can be well predicted using a thermodynamic model considering surfactant adsorption at the liquid-vapor (LV) and solid-liquid (SL) interfaces. At high C_S, however, all the DDAB drops wet on a Wenzel mode. Based on a Gibbsian thermodynamic analysis, we find that for the two types of superhydrophobic surfaces used, Wenzel state has the lowest thermodynamic energy and thus is more favorable theoretically. The CB state, however, is metastable at low C_S due to a thermodynamic energy barrier. The metastable CB wetting state becomes more stable on the SH microtextures with greater ϕ and r, in agreement with our experimental observations. Finally, we generalize this surface-energy analysis adopted to provide useful designs of surface parameters for a DDAB-laden surfactant droplet on the SH surface with a stable and robust CB state.

Introduction

The wetting and spreading characteristics of pure liquids on solid surfaces is of significant interest in several engineering and industrial applications, including droplet-based microfluidics,[1,2] coating,[3] inkjet or electrohydrodynamic jet printing,[4] and membranes technology, especially for oil-water separation.[5,6] In the past two decades, droplet wetting on low-energy surfaces, as so-called ultrahydrophobic or superhydrophobic (SH) surfaces with water contact angle (CA) ($\theta \geq 150°$) and small contact angle hysteresis (CAH), has received a great interest due to their promising applications for friction control, anti-icing, anti-fouling, self-cleaning, and improving corrosion resistance.[7–16] Such surfaces are not only chemically hydrophobic but also physically rough, consisting of both micro/nano-scaled roughness or structures. These useful SH surfaces allow the drop to sit on the top of the surface textures with air trapped underneath with a partial gas-liquid interface, as the so-called Cassie-Baxter (CB) or "Fakir" wetting state.[17,18]

The presence of a gas layer minimizes the interfacial energy, thereby making a CB state more favorable by reducing the contact area between the liquid and solid phases. However, the long-term stability of the preferred CB state on SH surfaces is still challenging and can be lost through an irreversible wetting transition to Wenzel (W) state, where the liquid fills in the surface cavities, when exposed to chemical,[19] high temper-

ature environment,[20,21] surfactant additives,[22] or evaporation.[23,24] To date, the wetting properties of SH surfaces have been extensively investigated, but mostly limited to pure liquids.[3,7–16,18,24–28] In contrast, amphiphilic aqueous surfactant solutions have been investigated to a less extent on SH surfaces, and there are only a handful experimental studies reported CB-W transition of surfactant-laden drops on SH surfaces.[29–39]

In this work, we investigate experimentally and theoretically how a cationic surfactant and its concentration changes the contact angle (CA) and wetting state of a droplet on ultra-hydrophobic microstructures of different solid-fraction (ϕ) and surface roughness (r). Systematic measurements of both CA and wetting states were conducted for nine DDAB surfactant concentrations. We compare our experimental results with thermodynamic predictions that consider surfactant adsorption at interfaces to examine C_S-dependent CA. Using Gibbsian thermodynamic analysis, we also elucidate theoretically the probability and the stability of the experimentally observed CB state at low C_S.

Experimental

Sample Preparation and Materials

Transparent polydimethylsiloxane (PDMS) microstructured SH surfaces with a square array of parallel cylindrical pillars (of height $H = 4.8\ \mu$m) were prepared using a replica modeling process.[24] Two pattern diameters (D) and pitches (P): $D = 4.9\ \mu$m, $P = 7.5\ \mu$m (surface S1) and $D = 4.6\ \mu$m, $P = 14.5\ \mu$m (surface S2) were used to obtain different ϕ and r (see Fig.1). The packing fraction, $\phi = \frac{\pi D^2}{4P^2}$, is the ratio of the liquid-solid surface area (pillar-top area) to the total (liquid-solid and liquid-gas) areas, and surface roughness, $r = 1 + \frac{\pi DH}{P^2}$, is the ratio of the total surface area to the projected one (on a 2D plane). In other words, r describes the relative change in the liquid-solid area for a rough surface compared to a flat surface in a Wenzel state,[40] while ϕ describes the percentage of the liquid–solid contact area in a Cassie–Baxter case.[17]

The surfactant solutions were prepared by dissolving didodecyldimethylammonium bromide (DDAB) powders (Sigma-Aldrich, 98%, with a critical micelle concentration (CMC) of = 0.085 mM) in ultrapure Milli-Q water (PURELAB Ultra, resistivity: 18.2 MΩ.cm) for nine different normalized concentrations, $C_S = C/\text{CMC} = 0$, 0.02, 0.05, 0.1, 0.2, 0.25, 0.5, 0.75, and 1, where C is DDAB surfactant concentration, and C_S is the normalized surfactant concentration by the critical micelle concentration (CMC). All solutions were prepared in glass beakers that were first cleaned with acetone, subsequently with ethanol, and finally rinsed thoroughly with Milli-Q water.

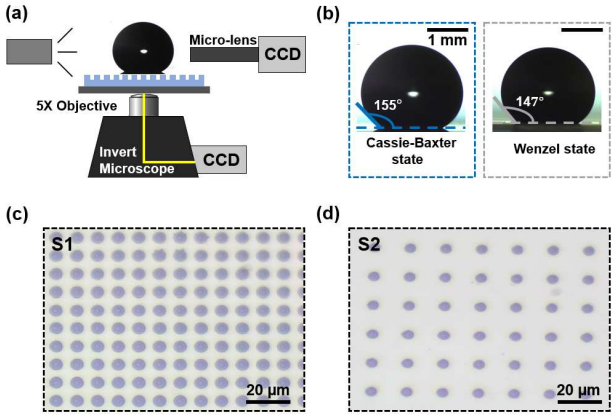

Figure 1. Schematic of the experimental setup in (a). (b) Different initial wetting states: side-view of a DDAB-laden droplets of $C_S = 0.1$ resting on a SH surface of $r = 1.33$, $\phi = 0.08$ (S2) in a CB state and in a W state, respectively. (c-d) Microscopic images of the two types of superhydrophobic microstructures used, with a square pillar pattern with a pillar diameter (D) and pitch (P), first, $r = 2.31$, $\phi = 0.34$ (for the SH S1 surface) in (c), and second, $r = 1.33$, $\phi = 0.08$ (for the SH S2 surface) in (d), respectively.

Wetting Experiments

For each surfactant concentration, ten drops were gently deposited using a 10 μl micro-pipette on each freshly made microstructured SH and flat PDMS surfaces. Two synchronized cameras were used to record the side and bottom views of the droplets upon deposition at 1 fps (frame per second). The side-view was recorded using a CCD camera (Thorlabs DCC3240C) coupled with a long-range magnifying lens (Navitor 12×) and the bottom-view using a color camera (Axiocam 105) integrated into an inverted microscope (Zeiss, with

a 5× objective). To measure the contact angles, we first extracted the shape of droplets from the side-view snapshots for the first and last 10 s of a 100 s acquisition period using ImageJ software.[41] Subsequently, a Matlab code based on axisymmetric drop shape analysis (ADSA) method was applied to measure the contact angle (θ).[25,42–44] Advancing and receding contact angles were also measured using the sessile drop method by slowly increasing and decreasing the droplet volume on the surface, respectively. Drop wetting states were determined through the bottom-view snapshots (see Fig. 2). All experiments were performed under ambient temperature (24 °C) at 1 atm and relative humidity of 29 ± 3%.

Theoretical

Contact angle models

To investigate the dependence of CAs and wetting states on the normalized cationic surfactant concentration, C_S, we follow a thermodynamic model proposed by Milne et al.[45] studying SDS-surfactant drop (on a Teflon SH surface). This theory combines the Gibbs adsorption equation, Young's, Cassie-Baxter, and Wenzel equations with adsorption isotherm to explain the effect of surfactant adsorption at each interface, which subsequently will influence the thermodynamic CAs. Firstly, the Gibbs adsorption describes the differential change in surface energy with a differential change in a surfactant concentration (C_S) in the aqueous solution:

$$d\gamma_{xy} = -\Gamma_{xy}\mathcal{R}T d\ \ln\ (C_S), \tag{1}$$

where γ_{xy} is the interfacial tension, Γ_{xy} is the surface coverage per unit area of surfactant at the interface xy (x and y represent a liquid (L) solid (S), or vapor (V) phase), $\mathcal{R}$ is the universal gas constant, T is the absolute temperature, and C_S is the non-dimensional surfactant concentration.

To compute Γ_{xy}, we use general isotherm equation proposed by Zhu-Gu[46] including Langmuir-type (L), S-type (S) and two plateaux- type (LS) adsorption isotherms. This general isotherm can be applied to liquid-vapor (LV), solid-liquid (SL), and solid-vapor (SV) interfaces, but here we assume no adsorption at the solid–vapor interface (i.e., $\Gamma_{SV} = 0$). The adsorption isotherm, Γ_{xy}, is:

$$\Gamma_{xy} = \Gamma_{xy}^{\infty}\frac{K_{xy}C_S^{n_{xy}}}{1 + K_{xy}C_S^{n_{xy}}}, \tag{2}$$

where Γ_{xy}^{∞} is the maximum surfactant concentration at the interface, K_{xy} is the equilibrium constant for adsorption, and n_{xy} is known as an empirical fitting parameter in the Zhu–Gu[46] adsorption isotherm.

By coupling the Gibbs adsorption equation (eq. (1)) with Zhu-Gu[46] adsorption isotherm (eq.(2)) and integrating at the LV interface, one obtains an expression for LV interfacial tension γ_{LV} as a function of surfactant concentration, C_S:

$$\gamma_{LV}(C_S) = \gamma_{LV}^{0} - \frac{\Gamma_{LV}\mathcal{R}T}{n_{LV}}\ln\ (1 + K_{LV}C_S^{n_{LV}}), \tag{3}$$

where γ_{LV}^{0} is the LV interfacial tension of pure water, i.e., for $C_S = 0, \Gamma_{LV}$ is the maximum surfactant concentration at the LV interface, $\mathcal{R}$ is the universal gas constant, T is the absolute temperature, K_{LV} is the adsorption equilibrium constant, and n_{LV} is an empirical fitting parameter. These LV adsorption parameters (Γ_{LV}, K_{LV}, and n_{LV}) are obtained by fitting eq. (3) to the experimental data of surface tension as a function of DDAB concentration,[47,48] i.e., $\gamma_{LV}(C_S)$.

To account for the surfactant adsorption on the SL interface, we applied a similar approach by solving Young's equation:[49] $\cos\theta_Y = (\gamma_{SV} - \gamma_{SL})/\gamma_{LV}$, where γ_{SV}, γ_{SL}, and γ_{LV} are the interfacial tension at the SV, SL, and LV interfaces, respectively. Using the Gibbs adsorption, i.e., eq. (1) and Zhu-Gu eq. (2) for the SL and LV interfaces, one can arrive at a modified Young equation[45] depending on surfactant concentration:

$$\theta_Y(C_S) = \cos^{-1}\left(\frac{\cos\theta_Y^{0}\gamma_{LV}^{0} + \frac{\Gamma_{SL}^{\infty}\mathcal{R}T}{n_{SL}}\ln\ (1 + K_{SL}C_S^{n_{SL}})}{\gamma_{LV}^{0} - \frac{\Gamma_{LV}^{\infty}\mathcal{R}T}{n_{LV}}\ln\ (1 + K_{LV}C_S^{n_{LV}})}\right), \tag{4}$$

where θ_{LV}^{0} is the Young contact angle for pure liquid on flat PDMS. This modified Young equation relates the contact angle of a drop on flat homogeneous surface with C_S (i.e., $\theta_Y(C_S)$) and is used to fit our experimental data of $\theta_Y(C_S)$ on flat PDMS to compute the surfactant adsorption parameters

(i.e., Γ_{SL}, K_{SL}, and n_{SL}) at the SL interface (see SI Section 4 for the details regarding the data fitting).

Two classical models are widely used to describe the contact angle on rough, rigid, homogeneous, and chemically inert surfaces. On the one hand, Wenzel (W)[40] equation is applied when the liquid has fully penetrated the cavities of the surface: $\cos\theta_W = r\cos\theta_Y$, where θ_W is the Wenzel CA, and r is the surface roughness. On the other, when the liquid sits on top of the surface texture, with air trapped beneath the drop in the surface cavities, Cassie-Baxter (CB)[17] equation is used: $\cos\theta_{CB} = \phi\cos\theta_Y - (1-\phi)$, where θ_{CB} is CB CA and ϕ is the packing fraction of the liquid-solid surface area (pillar-top area) to the total (SL and LV) areas. To account for the surfactant adsorption for a drop on such rough surfaces, C_S, r and ϕ will affect surfactant adsorption since the surfactant molecules will adsorb to both the LV and SL interfaces. Following the same process by substituting the modified Young equation (eq.(4)) into the W and CB equations, we arrive in the forms of the Milne et al.[45] modified W and CB CA equations:

$$\theta_W(C_S) = \cos^{-1}\left(\frac{\cos\theta_W^0\gamma_{LV}^0 + r\frac{\Gamma_{SL}^\infty \mathcal{R}T}{n_{SL}}\ln\,(1+K_{SL}C_S^{n_{SL}})}{\gamma_{LV}^0 - \frac{\Gamma_{LV}^\infty \mathcal{R}T}{n_{LV}}\ln\,(1+K_{LV}C_S^{n_{LV}})}\right), \tag{5}$$

$$\theta_{CB}(C_S) = \cos^{-1}\left(\frac{\cos\theta_{CB}^0\gamma_{LV}^0 + \phi\frac{\Gamma_{SL}^\infty \mathcal{R}T}{n_{SL}}\ln\,(1+K_{SL}C_S^{n_{SL}}) + (1-\phi)\frac{\Gamma_{LV}^\infty \mathcal{R}T}{n_{LV}}\ln\,(1+K_{LV}C_S^{n_{LV}})}{\gamma_{LV}^0 - \frac{\Gamma_{LV}^\infty \mathcal{R}T}{n_{LV}}\ln\,(1+K_{LV}C_S^{n_{LV}})}\right), \tag{6}$$

where θ_W^0 and θ_{CB}^0 are the W and CB CAs for pure liquid on a rough surface and can be estimated using: $\cos\theta_W^0 = r\cos\theta_Y^0$ and $\cos\theta_{CB}^0 = \phi\cos\theta_Y^0 - (1-\phi)$, respectively. Here, θ_Y^0 is the Young CA for pure water on a flat PDMS surface, $\mathcal{R}$ is the universal gas constant, T is the absolute temperature, Γ_{LV}^∞ and K_{LV} are Zhu–Gu[46] adsorption parameters that describe the maximum surfactant concentration at the LV interface and the equilibrium constant for adsorption, respectively. Γ_{SL}^∞ and K_{SL} represent similar quantities but for the SL interface, and n_{LV} and n_{SL} are empirical fitting parameters in the Zhu–Gu[46] adsorption isotherm.

Eqs. (4) - (6) are predictive equations to quantify the influence of DDAB surfactant adsorption at the LV and SL interfaces on the contact angle of the drops on flat and textured surfaces (characterized by ϕ and r). In terms of physical mechanisms, the first term in the numerator in eq. (5) and eq. (6) describes the effect of the surface roughness and the solid-fraction on the CA of pure water. The second term in the numerator expresses the effect of surfactant adsorption on the SL interface. The third term in the numerator in the modified CB equation and the denominator for both modified W and CB equations describe the effect of surfactant adsorption on the LV interface as a function of C_S in determining the contact angle on textured surfaces. It is worth noting that we have not considered any pinning effects for both CB and W contact angles. On the one hand, such theoretical prediction for a Wenzel state, usually with pinning contact line, can contribute to some errors, and has shown a deviation from the experimental data by previous studies using SDS surfactants.[45] On the other hand, such consideration without a contact line pinning is acceptable for predicting a CB contact angle since the CB mode generally accompanies with high CAs and high mobility.[50] In addition, to the best of our knowledge, no predictive theory for the pinning of the contact line in the CB state is available.

Results and Discussion

Wetting states

Figure 2 shows the side and bottom-view snapshots on both superhydrophobic microstructures

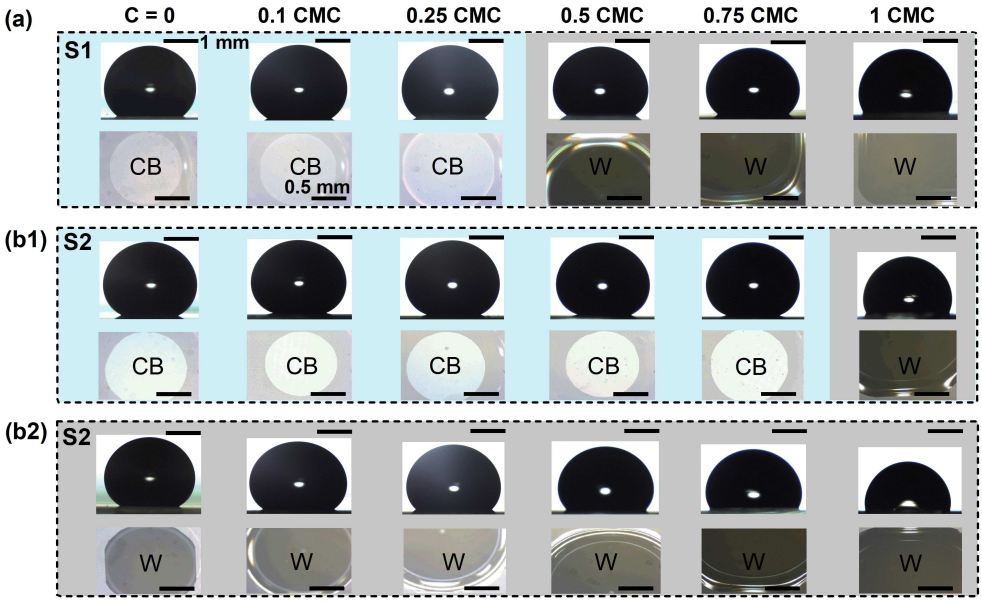

Figure 2. Side- and bottom-view snapshots of drops with different surfactant concentrations of DDAB, C (0 to 1 CMC), on the SH microstructured surface S1 ($r = 2.31$, $\phi = 0.34$) in (a) and surface S2 ($r = 1.33$, $\phi = 0.08$) in (b1 and b2), showing a transition from Cassie–Baxter (CB) to Wenzel (W) wetting at high DDAB concentration. Both DDAB concentration and the surface parameters influence the wetting state. On one hand, as revealed in (a), DDAB drops on the high-r SH surface (S1) were always in a gas-trapping CB state at low C (of $C = 0$ to 0.25 CMC) and a Wenzel state at high C. On the other, we observed that low-C drops (of $C = 0$ to 0.75 CMC) can sometimes form a CB, as shown in (b1), or a Wenzel state, as revealed in (b2), on the lower-r SH (S2). At 1 CMC, all drops were in a W mode.

(surfaces S1 and S2) with two distinct wetting states: Cassie-Baxter (CB) and Wenzel (W). To distinguish between these states, a bright contact area at the center was observed when the drop sitting on top of the surface roughness with air underneath, representing a CB drop. In contrast, a dark central, contact area was observed when water completely wets the surface structure as in a Wenzel state. Such color contrast (bright vs. dark) between the CB and Wenzel wetting is caused by the different refractive indices between air and water.

Our results shown in Fig. 2 reveal that drops were in a CB state when C_S between 0 and 0.25 on the higher-r SH surface S1 ($r = 2.31$, $\phi = 0.34$) but in a W state when C_S ranges from 0.5 to 1 (Fig. 2a). On the lower-r SH surface S2 ($r = 1.33$ and $\phi = 0.08$), with 9-10 independent experiments, we observed that DDAB drops of C_S between 0 and 0.75 can sometimes form a CB or a Wenzel wetting state, while their representative experimental snapshots are shown in Fig. 2(b1) and 2(b2), respectively. At 1 CMC, DDAB drops were always in a Wenzel wetting state for both SH surfaces, S1 and S2. We discuss and explain the probability for the presence of different wetting states (being a CB or Wenzel state) experimentally and theoretically in the later sections. In brief, depending on the surface parameters, r and ϕ, there is a wetting transition from a CB to W wetting state of DDAB drops with increasing C_S for both SH surfaces.

C_S-dependent contact angles

Fig. 3 shows the experimental and theoretical results for the C_S-dependent CAs of CB and W drops on both SH surfaces: S1 (◆) and S2 (●). The CAs of CB drops on the SH microstructures, S1 (◆) and S2 (●), were almost constant regardless of the change in C_S. However, the CAs decreases with increasing C_S for Wenzel drops and reach a minimum value of $\theta \simeq 100^\circ$ and $\theta \simeq 80^\circ$ for S1 (◇) and S2 (□), respectively. The theoretical predictions were estimated using the modified W and CB equations, i.e., eq. (5) and (6). As revealed in Fig. 3, there is a good agreement between our experimental data (filled symbols) and the predictions (solid lines, eq. (6)) of the C_S-dependent

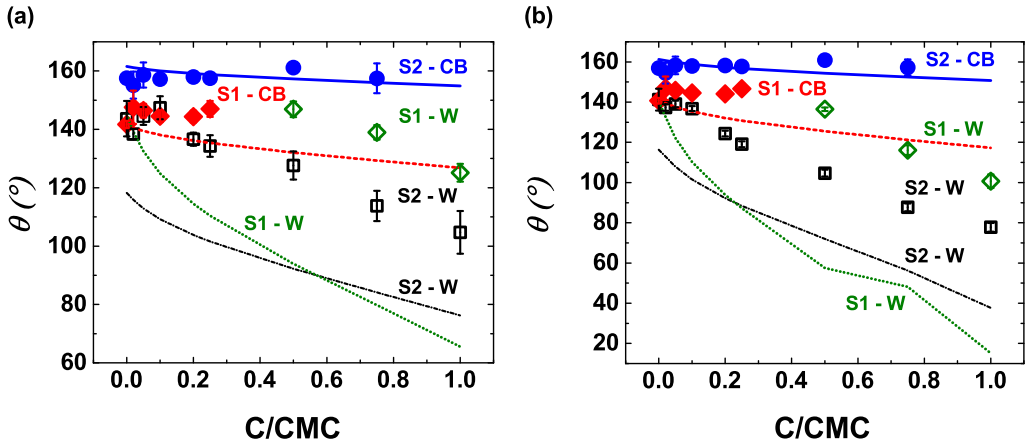

Figure 3. Measured and predicted contact angles for DDAB droplets at concentrations between 0 and 1 CMC on two SH microstructures: high-r S1 and and low-r S2. The CA data were measured during the first 10 s in (a) and last 10 s in (b) of a period of 100 s right after the droplet deposition. Different symbols denote CB (◆) and W (◇) drops on the high-r S1, while CB (●) and W (□) drops on the low-r S2. The error bars represent the standard deviations of ten drops for each C_S. Theoretical prediction of the CB and W contact angles considering surfactant adsorption, given by eqs. (5)-(6), are also plotted for S1 (- - - ,⋯⋯) and S2 (——,-·-·-), respectively.

CAs of CB drops, particularly for the SH surface S2. This better agreement for the S2 may be attributed to the smaller solid fraction (lower ϕ) and, hence, less pinning of the contact line. Both measured and predicted CB CAs on the lower-ϕ S2 are larger compared to those on the higher-ϕ S1 due to greater liquid-air contact with smaller ϕ.

While there is a good agreement of the C_S-dependent contact angles of CB drop on both SH surfaces, the prediction using a modified W equation was not good for both S1 (⋯⋯) and S2 (-·-·-) surfaces (dashed lines in Fig. 3). This may be attributed to a larger deviation due to the pinning contact line whose effect was not considered in the theory for a Wenzel DDAB drop on the microstructures.[38,51] In addition, to get better predictions of the C_S-dependent CAs of W-state drops, one may need to include the contribution from pinning for W drops due to the greater solid-liquid contact area (higher ϕ).[51,52] It has been shown that the modified CB equation can predict the measurements of CB CAs successfully and can be expanded to other types of surfaces with different ϕ and r values as well as various surfactant solutions once the data of θ_Y and γ_{LV} are available.

Advancing and receding contact angles

The wetting behavior of DDAB surfactant drops on flat PDMS and both microstructured SH surfaces S1 and S2 is also investigated through the measurements of advancing (θ_{Adv}) and receding (θ_{Rec}) CAs as a function of C_S, shown in Fig. 4a and 4b, respectively. On higher-r S1, the advancing and receding CAs for pure water (C_S = 0) measured to be θ_{Adv} = 163.9 ± 2.2° and θ_{Rec} = 159.0 ± 1.4°, respectively. Both the advancing and receding CAs decrease with increasing C_S and reach a minimum value when C_S = 1 of θ_{Adv} = 139.3 ± 4.3° and θ_{Rec} = 103.9 ± 4.8°, respectively. The lower-ϕ and r S2, on the other hand, showed lower advancing and receding CAs of pure water θ_{Adv} = 145.8 ± 2.3° and θ_{Rec} = 136.5 ± 0.74°. We may attribute the lower advancing and receding CAs on S2 to a CB to Wenzel wetting transition, which occurs during the measurement and subsequently the liquid homogeneously wets on the surface textures resulting in a lower CA. Similarly, as C_S is increased, the advancing and receding CAs on S2 start to decrease when C_S > 0.5 and reach a minimum value at C_S =1 of θ_{Adv} = 121.6 ± 3.7° and θ_{Rec} = 91.7 ± 3.7°, respectively. Both surfaces S1 and S2 lost their superhydrophobicity with increasing C_S when C_S > 0.5 (Fig. 4a-b).

As shown in Fig. 4a, our measurement for the advancing CA on S2 reveals a good agreement

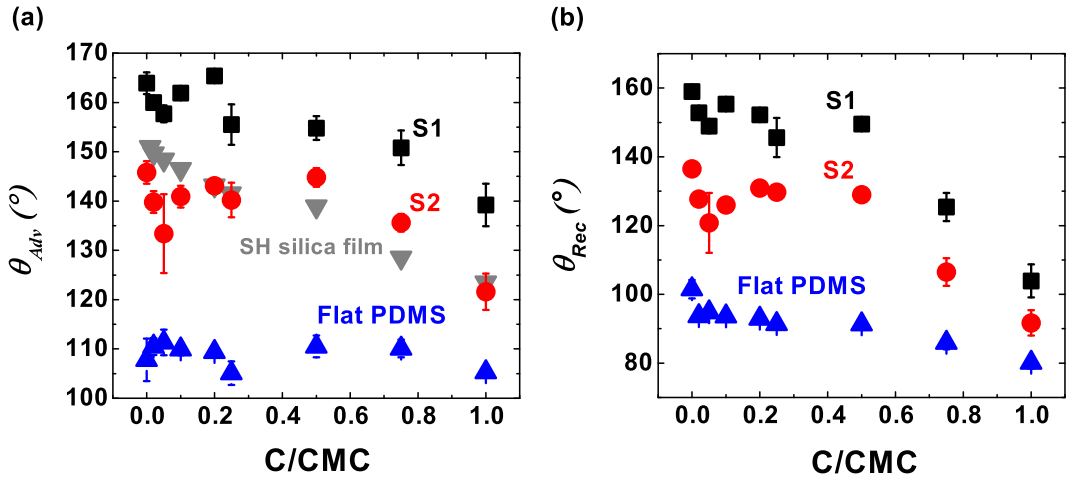

Figure 4. (a) Advancing and (b) receding contact angles measured for DDAB drops at for different concentrations between 0 and 1 CMC on three types of surfaces: Flat PDMS (▲), SH microstructures S1 (■) and S2 (●), using a sessile drop method by adding (or withdrawing) liquid to measure the advancing (or receding) CAs. Error bars show the standard deviations obtained from ten experiments. The advancing contact angles for DDAB drops on a SH silica-based thin film (▼) are plotted for comparison.[31]

with that on SH thin-film porous sol–gel surface (▼).[31] Finally, the advancing CAs on flat PDMS are nearly constant for C_S from 0 to 1, while the receding CAs reduce from $\theta_{Rec} = 101.5 \pm 2.7°$ at $C_S = 0$ to $\theta_{Rec} = 80.1 \pm 1.7°$ at $C_S = 1$.

Free energy analysis for the stability and metastability of the wetting states

Although the modified CB eq. (6) well predicted C_S-dependent CA for CB drops, it doesn't explain the probability and the stability of the wetting states (shown in Fig. 2). To get a better understanding concerning the stability and the metastability of the observed wetting behavior and to explain the occurrence of different wetting states depending on the C_S on the different microstructures, we carried out an analysis starting from the Gibbsian thermodynamics,[23,38,53–57] following the work by Shardt et al.[38] using SDS surfactants, and analytically estimated the free energy (E) for our composite system of DDAB-laden surfactant droplets sitting on a microstructured surface. The derived free energy equation, $E - E_0$, with respect to the assumed reference state has the form of Shardt et al.[38] free energy:

$$E - E_0 = \gamma_{LV}\pi R^2(2 - 3\cos\theta + \cos^3\theta) - 4\pi\gamma_{LV}R_0^2, \quad (7)$$

where E_0 is the free energy at the assumed reference state of a spherical drop without any SL contact; R is the spherical cap radius of curvature; R_0 is the initial radius of a spherical drop of 10 μl; $\cos\theta = f\cos\theta_Y(C_S) - f_1$. Here, f is the ratio of the SL surface area (pillar-top area) to the total (SL and LV) areas, and f_1 is the ratio of the LV interfacial area to the total projected area beneath the drop (See SI Section 3 for the derivation).

We followed a model that a droplet transiting from CB to W wetting state usually occurs through two main phases described below.[23,38,58] In this first phase, after droplet deposition, the liquid is falling down along the pillars with an assumed flat LV interface as in a CB wetting state (with $f = \phi$ and $f_1 = 1 - \phi$), until it wets the bottom of the surface. Here, we assume that only the cylinder's walls are wet and the bottom surface is not wet, so f increases and $f_1 = 1 - f$. At the end of the first phase, the value of f further increases as the solid–liquid contact area increases. In the second phase, liquid gradually wets the bottom surface from the pillar edges towards the center. In other words, f continues to increase until the bottom area is completely wetted with the liquid, while $f_1 = r - f$. A full transition to Wenzel wetting occurs when $f = r$ and $f_1 = 0$, where $\cos\theta = r\cos\theta_Y(C_S)$ as in the Wenzel eq.[17,23,40]

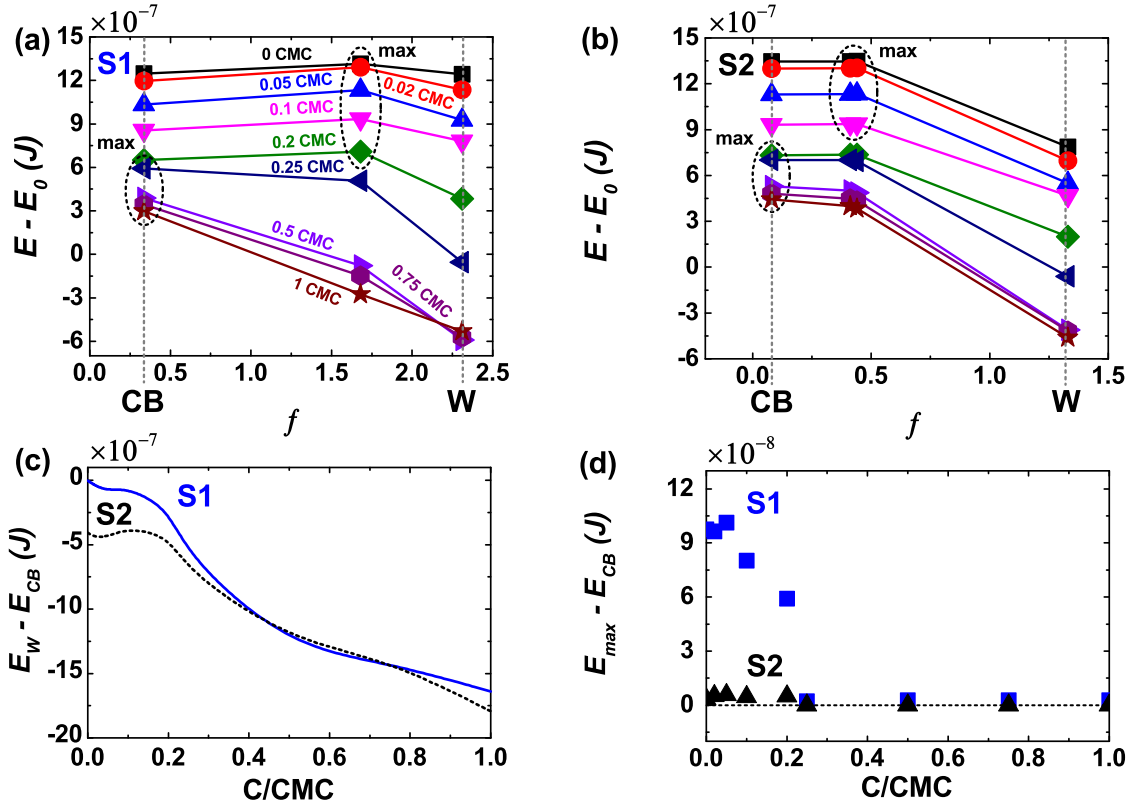

Figure 5. Free energy (E) with respect to the reference state (E_0) during the wetting transition of the drop from CB to W passing through the intermediate states where the drop partially wet the microstructures for 9 surfactant concentrations on SH surfaces S1 in (a) and S2 in (b). (c) The difference between the W and CB free energy as a function of $C_S = C/CMC$ is of the order of 10^{-7} J for S1 (——) and S2 (- - -). (d) The free energy barrier (i.e., the difference between the maximum free energy (E_{max}) and the CB free energy, $E_{max} - E_{CB}$, as a function of C_S for S1 (■) and S2 (▲).

Fig. 5 (a-b) shows the free energy, E, of DDAB-surfactant droplets with respect to the chosen reference state, E_0, for nine different values of C_S on the high-r SH surface S1 in (a) and low-r S2 in (b), as a function of f. Here f describes the depth of liquid penetration in between the pillars. On the one hand, for droplets with C_S from 0 to 0.2 CMC on both SH surfaces, the free energy first increases as f increases until the maximum free energy (E_{max}) is reached, and subsequently decreases to reach a minimum value of the free energy in a Wenzel state. On the other, for C_S between 0.25 and 1 CMC on both surfaces, the free energy of the DDAB drop initially starts from a maximum value at a CB state and continuously declined as f increases until the Wenzel state, which has lower free energy by $O(10^{-7}J)$ compared to that of the CB state. The difference in the free energy between W and CB as a function of C_S (Fig. 5c), $E_W - E_{CB} < 0$, reveals that Wenzel state is theoretically and thermodynamically preferred since E_W is the lowest, in agreement with the typical CB-W transition criterion observed previously for pure liquid.[18,23–25,59,60] However, based on the analysis there is a free energy barrier between the CB and W states, $E_{max} - E_{CB} > 0$ (see Fig. 5d), to be overcome for a drop to transient to W state for both SH surfaces at $0 \lesssim C_S \lesssim 0.25$. In other words, the CB is metastable due to the free energy barrier at these concentrations (See SI for the derivation).

The predicted free energy barrier, $E_{max} - E_{CB} > 0$, for the higher-r S1 (■) is relatively higher when $C_S \leq 0.25$, of the order of magnitude of $O(10^{-8} - 10^{-7}J)$ (shown in Fig. 5d), and is consistent with our experimental observations that all DDAB drops are in a CB state on S1 (revealed in 6a). The presence of the high energy barrier for S1 makes a CB state thermodynamically more favourable at these concentrations. In contrast, due to the lower energy barrier of $O(10^{-8}J)$ for low-r

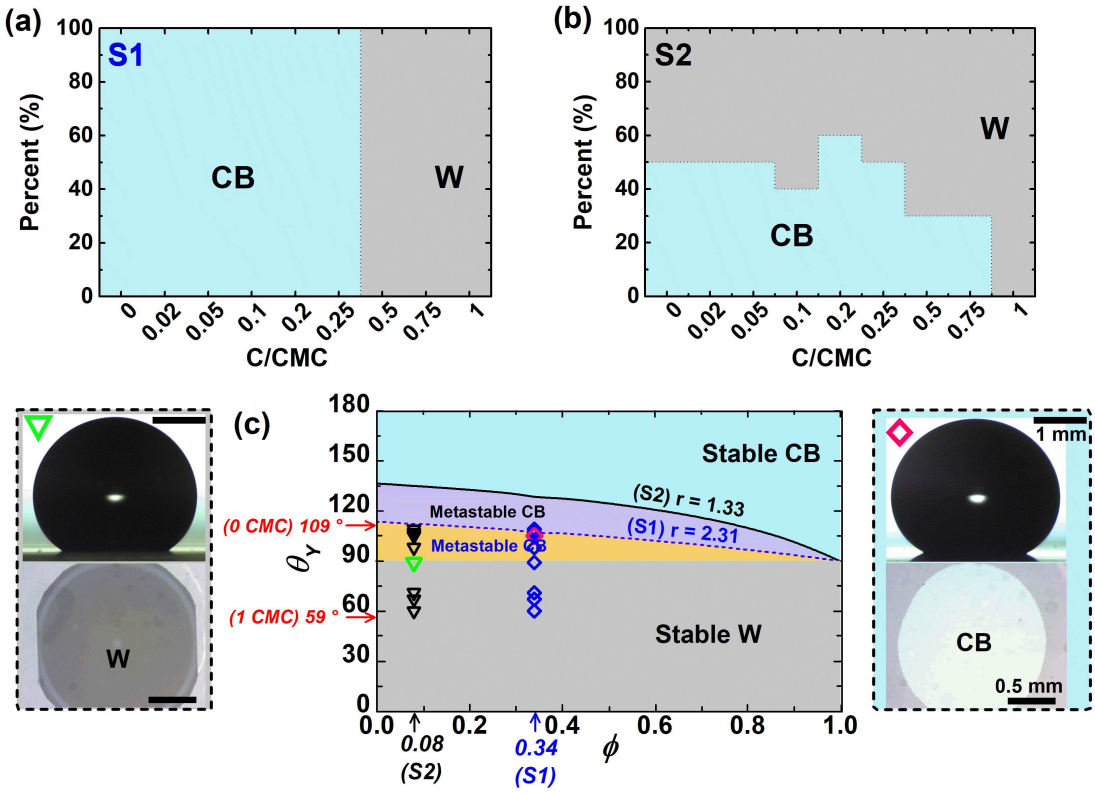

Figure 6. Percentage of experimental droplets in a Cassie-Baxter (CB) and Wenzel (W) state as a function of normalized surfactant concentration (C_S) for high-r S1 in (a) and low-r S2 in (b), based on an average of ten independent droplets for each DDAB surfactant concentration. (c) Phase diagram of CB and W wetting states based on the free energy analysis eq. (7) as a function of the solid-liquid fraction (ϕ) and the Young's modified contact angle on a Flat PDMS, $\theta_Y(C_S)$ for two different surface roughnesses (r). Symbols show the modeled CAs for the experimental parameters of r and ϕ for the SH S1 (◇) and S2 (▽) for C_S between 0 and 1 CMC, while $\theta_Y(C_S = 0)$ = 109° and $\theta_Y(C_S = 1)$ = 59° for DDAB-laden droplets. Side- and bottom-view snapshots showed a stable W (Left, ▽) and a metastable CB (Right, ◇) drops, respectively. In (c), the critical boundaries delineating the stable CB and Wenzel states are depicted by the lines for both S1 (- - -) and S2 (—), using the criteria derived, namely $\cos\theta^*_Y(C_S) = \left(\frac{\phi-1}{r-\phi}\right)$.

SH S2 (shown in Fig. 5d), some droplets were observed to be in a CB state while some at a Wenzel wetting state for C_S between 0 and 0.75 CMC. Fig. 6b shows the respective probability of a CB or W wetting state observed based on ten independent experiments. At high C_S = 1 CMC, a W state was observed on both surfaces.

Apart from our two types of SH surfaces investigated, we provide a layout of optimal r and ϕ for designing robust SH surfaces with a stable CB state that has various beneficial applications such as self-cleaning. By equating $E_{CB} = E_W$ using eq. (7), one can arrive at the physical criterion of the critical modified Young's contact angle for a surfactant-laden droplet, θ^*_Y, which delineates the surface parameters for a stable CB *vs.* Wenzel state: $\cos\theta^*_Y = (\frac{\phi-1}{r-\phi})$.[25,59,60] In the phase diagram shown in Fig. 6c, using this method we summarize the thermodynamic stability predictions of wetting states depending on C_S, θ_Y, ϕ, and r. A stable CB region is predicted for a large $\theta_Y < \cos^{-1}\left(\frac{\phi-1}{r-\phi}\right)$, whereas a stable Wenzel state occurs for small θ_Y ($\leq 90°$) in Fig. 6c.

To examine the occurrence of metastable CB state in our experiments, we used a theoretical criteria based on the differential of the free energy barrier with respect to f, i.e., $\partial E/\partial f|_{f=\phi} > 0$.[38,58] From Fig. 6c and using such criterion, we can conclude that for the metastable CB state to appear, θ_Y should be greater than 90°, while a Wenzel state is thermodynamically stable for all ϕ and r with a small $\theta_Y \leq 90°$. In addition, the metastable CB

region for S1 extends from $\theta_Y = 90^\circ$ to the blue dashed line (orange area), while that for S2 expands from $\theta_Y = 90^\circ$ to the black solid line and overlaps with the metastable CB region for S1. These are in agreement with our experimental observations, where W states appeared at higher C_S (i.e., low θ_Y) and metastable CB states observed for lower C_S (i.e., high θ_Y).

Conclusion

In summary, we experimentally measured the contact angles and wetting states of DDAB surfactant-laden drops for nine different concentrations on two types of superhydrophobic microstructures of different packing-fraction (ϕ) and surface roughness (r). A model considering surfactant adsorption at the LV and SL interfaces has been derived and compared to these experimental data. The experimental data and the theoretical predictions of the CB contact angles were in good agreement. However, the theoretical prediction using a modified W equation didn't predict well the Wenzel contact angles for both surfaces, likely due to the pinning effects of the wetting contact line. We further consider thermodynamic surface energies to predict the stability or metastability of the wetting states depending on C_S. We found that the Wenzel state is thermodynamically favorable for both SH surfaces at all DDAB concentrations, but there is a free energy barrier between the CB and W states for $C_S \leq 0.25$ for our SH surfaces. This thermodynamic analysis implies that the CB state is metastable at these concentrations and, moreover, this metastable CB state becomes more stable on surfaces with greater ϕ and r. Based on the free energy barrier and the adsorption thermodynamics for surfactant-laden drops, we highlight the prediction of a stable and robust gas-trapping, CB state superhydrophobic microstructures beneficial for various applications of self-cleaning and low-friction, when meeting the following two criteria: first, a large Young contact angle of a surfactant-laden drop on the flat surface: $\theta_Y(C_S) > 90^\circ$ and, second, large values of r and ϕ which satisfy $\cos\theta_Y(C_S) < (\frac{\phi-1}{r-\phi})$.

Acknowledgement The authors thankfully acknowledge useful discussion with Drs. N. Shardt and J.A.W. Elliots. P.A.T holds a Canada Research Chair in Fluids and Interfaces and gratefully acknowledges funding from the Natural Sciences and Engineering Research Council of Canada (NSERC) and Alberta Innovates.

Supporting Information

See the supplementary document for more details about the experimental data, the fitting parameters used, free energy derivation, and the derivation of the criterion that defines the stability and the metastability of a Cassie–Baxter wetting state.

References

(1) Baret, J.-C. Surfactants in droplet-based microfluidics. Lab Chip **2012**, 12, 422–433.

(2) Xu, J.; Dong, P.; Zhao, H.; Tostado, C.; Luo, G. The dynamic effects of surfactants on droplet formation in coaxial microfluidic devices. Langmuir **2012**, 28, 9250–9258.

(3) Lomga, J.; Varshney, P.; Nanda, D.; Satapathy, M.; Mohapatra, S.; Kumar, A. Fabrication of durable and regenerable superhydrophobic coatings with excellent self-cleaning and anti-fogging properties for aluminium surfaces. J. Alloys Compd. **2017**, 702, 161–170.

(4) Park, J. U.; Hardy, M.; Kang, S. J.; Barton, K.; Adair, K.; Mukhopadhyay, D. K.; Lee, C. Y.; Strano, M. S.; Alleyne, A. G.; Georgiadis, J. G.; Ferreira, P. M.; Rogers, J. A. High-resolution electrohydrodynamic jet printing. Nat. Mater. **2007**, 6, 782–789.

(5) Koh, J. J.; Lim, G. J.; Zhou, X.; Zhang, X.; Ding, J.; He, C. 3D-Printed Anti-Fouling Cellulose Mesh for Highly Efficient Oil/Water Separation Applications. ACS Appl. Mater. Interfaces **2019**, 11, 13787–13795.

(6) Lv, J.; Gong, Z.; He, Z.; Yang, J.; Chen, Y.; Tang, C.; Liu, Y.; Fan, M.; Lau, W.-M. 3D printing of a mechanically durable superhydrophobic porous membrane for oil–

water separation. J. Mater. Chem. A **2017**, 5, 12435–12444.
(7) Rothstein, J. P. Slip on superhydrophobic surfaces. Annu. Rev. Fluid Mech. **2010**, 42, 89–109.
(8) Bocquet, L.; Lauga, E. A smooth future? Nat. Mater. **2011**, 10, 334–337.
(9) Karatay, E.; Haase, A. S.; Visser, C. W.; Sun, C.; Lohse, D.; Tsai, P. A.; Lammertink, R. G. Control of slippage with tunable bubble mattresses. PNAS **2013**, 110, 8422–8426.
(10) Kreder, M. J.; Alvarenga, J.; Kim, P.; Aizenberg, J. Design of anti-icing surfaces: smooth, textured or slippery? Nat. Rev. Mater. **2016**, 1, 1–15.
(11) Sarshar, M. A.; Swarctz, C.; Hunter, S.; Simpson, J.; Choi, C.-H. Effects of contact angle hysteresis on ice adhesion and growth on superhydrophobic surfaces under dynamic flow conditions. Colloid Polym. Sci. **2013**, 291, 427–435.
(12) Xue, C.-H.; Guo, X.-J.; Ma, J.-Z.; Jia, S.-T. Fabrication of robust and antifouling superhydrophobic surfaces via surface-initiated atom transfer radical polymerization. ACS Appl. Mater. Interfaces **2015**, 7, 8251–8259.
(13) Lai, Y.; Tang, Y.; Gong, J.; Gong, D.; Chi, L.; Lin, C.; Chen, Z. Transparent superhydrophobic/superhydrophilic TiO 2-based coatings for self-cleaning and anti-fogging. J. Mater. Chem. **2012**, 22, 7420–7426.
(14) Kulinich, S.; Farhadi, S.; Nose, K.; Du, X. Superhydrophobic surfaces: are they really ice-repellent? Langmuir **2010**, 27, 25–29.
(15) Drelich, J.; Chibowski, E.; Meng, D. D.; Terpilowski, K. Hydrophilic and superhydrophilic surfaces and materials. Soft Matter **2011**, 7, 9804–9828.
(16) Bagheri, H.; Aliofkhazraei, M.; Forooshani, H. M.; Rouhaghdam, A. S. Electrodeposition of the hierarchical dual structured (HDS) nanocrystalline Ni surface with high water repellency and self-cleaning properties. J. Taiwan Inst. Chem. Eng. **2017**, 80, 883–893.
(17) Cassie, A.; Baxter, S. Wettability of porous surfaces. J. Chem. Soc. Faraday Trans. **1944**, 40, 546–551.
(18) Quéré, D. Non-sticking drops. Rep. Prog. Phys. **2005**, 68, 2495–2532.
(19) Cai, P.; Bai, N.; Xu, L.; Tan, C.; Li, Q. Fabrication of superhydrophobic wood surface with enhanced environmental adaptability through a solution-immersion process. Surf. Coatings Technol. **2015**, 277, 262–269.
(20) Guo, P.; Zhai, S.; Xiao, Z.; An, Q. One-step fabrication of highly stable, superhydrophobic composites from controllable and low-cost PMHS/TEOS sols for efficient oil cleanup. J. Colloid Interface Sci. **2015**, 446, 155–162.
(21) Heinonen, S.; Huttunen-Saarivirta, E.; Nikkanen, J.-P.; Raulio, M.; Priha, O.; Laakso, J.; Storgårds, E.; Levänen, E. Antibacterial properties and chemical stability of superhydrophobic silver-containing surface produced by sol–gel route. Colloids Surfaces A Physicochem. Eng. Asp. **2014**, 453, 149–161.
(22) Farhadi, S.; Aliofkhazraei, M.; Darband, G. B.; Abolhasani, A.; Rouhaghdam, A. S. Corrosion and wettability of PEO coatings on magnesium by addition of potassium stearate. J. Magnes. Alloy. **2017**, 5, 210–216.
(23) Ishino, C.; Okumura, K.; Quéré, D. Wetting transitions on rough surfaces. EPL **2004**, 68, 419–425.
(24) Tsai, P.; Lammertink, R. G.; Wessling, M.; Lohse, D. Evaporation-triggered wetting transition for water droplets upon hydrophobic microstructures. Phys. Rev. Lett. **2010**, 104, 2–3.
(25) Bussonnière, A.; Bigdeli, M. B.; Chueh, D.-Y.; Liu, Q.; Chen, P.; Tsai, P. A. Universal wetting transition of an evaporating water droplet on hydrophobic micro-and nanostructures. Soft matter **2017**, 13, 978–984.
(26) Tie, L.; Guo, Z.; Liang, Y.; Liu, W. Water super-repellent behavior of semicircular micro/nanostructured surfaces. Nanoscale **2019**, 11, 3725–3732.
(27) Wu, H.; Jiang, K.; Xu, Z.; Yu, S.; Peng, X.; Zhang, Z.; Bai, H.; Liu, A.; Chai, G. Theoretical and Experimental Studies on the Controllable Pancake Bouncing Behavior of Droplets. Langmuir **2019**, 35, 17000–17008.

(28) Yu, Y.-S.; Huang, X.; Sun, L.; Zhou, J.-Z.; Zhou, A. Evaporation of ethanol/water mixture droplets on micro-patterned PDMS surfaces. Int. J. Heat Mass Transf. **2019**, 144, 118708.
(29) Mohammadi, R.; Wassink, J.; Amirfazli, A. Effect of surfactants on wetting of superhydrophobic surfaces. Langmuir **2004**, 20, 9657–9662.
(30) Ferrari, M.; Ravera, F.; Rao, S.; Liggieri, L. Surfactant adsorption at superhydrophobic surfaces. Appl. Phys. Lett. **2006**, 89, 053104.
(31) Chang, F.-M.; Sheng, Y.-J.; Chen, H.; Tsao, H.-K. From superhydrophobic to superhydrophilic surfaces tuned by surfactant solutions. Appl. Phys. Lett. **2007**, 91, 1–4.
(32) Ferrari, M.; Ravera, F.; Liggieri, L. Wetting of single and mixed surfactant solutions on superhydrophobic surfaces. J Adhes Sci Technol **2009**, 23, 483–492.
(33) Ferrari, M.; Ravera, F. Surfactants and wetting at superhydrophobic surfaces: Water solutions and non aqueous liquids. Adv. Colloid Interface Sci. **2010**, 161, 22–28.
(34) Shirtcliffe, N. J.; McHale, G.; Newton, M. I. Wet adhesion and adhesive locomotion of snails on anti-adhesive non-wetting surfaces. PloS One **2012**, 7, 5–9.
(35) Milne, A.; Elliott, J.; Amirfazli, A. Contact angles of surfactant solutions on heterogeneous surfaces. Phys. Chem. Chem. Phys. **2015**, 17, 5574–5585.
(36) Zhu, Y.; Gao, Y.; Zhang, C.; Zhao, X.; Ma, Y.; Du, F. Static and dynamic wetting behavior of TX-100 solution on superhydrophobic rice (Oryza sativa.) leaf surfaces. Colloids Surf. A Physicochem. Eng. Asp. **2018**, 547, 148–156.
(37) Zhang, C.; Zhao, X.; Lei, J.; Ma, Y.; Du, F. The wetting behavior of aqueous surfactant solutions on wheat (Triticum aestivum) leaf surfaces. Soft Matter **2017**, 13, 503–513.
(38) Shardt, N.; Bigdeli, M. B.; Elliott, J. A.; Tsai, P. A. How Surfactants Affect Droplet Wetting on Hydrophobic Microstructures. J. Phys. Chem. Lett. **2019**, 10, 7510–7515.
(39) Thiele, U.; Snoeijer, J. H.; Trinschek, S.; John, K. Equilibrium contact angle and adsorption layer properties with surfactants. Langmuir **2018**, 34, 7210–7221.
(40) Wenzel, R. N. Resistance of solid surfaces to wetting by water. Ind. Eng. Chem. **1936**, 28, 988–994.
(41) Schneider, C. A.; Rasband, W. S.; Eliceiri, K. W. NIH Image to ImageJ: 25 years of image analysis. Nat. Methods **2012**, 9, 671–675.
(42) Del Río, O.; Neumann, A. Axisymmetric drop shape analysis: computational methods for the measurement of interfacial properties from the shape and dimensions of pendant and sessile drops. J. Colloid Interface Sci. **1997**, 196, 136–147.
(43) Wege, H. A.; Holgado-Terriza, J. A.; Rosales-Leal, J. I.; Osorio, R.; Toledano, M.; Cabrerizo-Vílchez, M. Á. Contact angle hysteresis on dentin surfaces measured with ADSA on drops and bubbles. Colloids Surfaces A Physicochem. Eng. Asp. **2002**, 206, 469–483.
(44) Hoorfar, M.; Neumann, A. Axisymmetric drop shape analysis (ADSA) for the determination of surface tension and contact angle. J. Adhes. **2004**, 80, 727–743.
(45) Milne, A.; Elliott, J.; Zabeti, P.; Zhou, J.; Amirfazli, A. Model and experimental studies for contact angles of surfactant solutions on rough and smooth hydrophobic surfaces. Phys. Chem. Chem. Phys. **2011**, 13, 16208–16219.
(46) Zhu, B.-Y.; Gu, T. General isotherm equation for adsorption of surfactants at solid/liquid interfaces. Part 1. Theoretical. J. Chem. Soc., Faraday Trans. I **1989**, 85, 3813–3817.
(47) Biswal, N. R.; Paria, S. Interfacial and wetting behavior of natural–synthetic mixed surfactant systems. RSC Advances **2014**, 4, 9182–9188.
(48) Biswal, N. R.; Paria, S. Wetting of PTFE and glass surfaces by aqueous solutions of cationic and anionic double-chain surfactants. Ind. Eng. Chem. Res. **2012**, 51, 10172–10178.
(49) Young, T. III. An essay on the cohesion of fluids. Philos. Trans. Royal Soc. **1805**, 95, 65–87.
(50) Pierce, E.; Carmona, F.; Amirfazli, A. Understanding of sliding and contact angle results

in tilted plate experiments. Colloids Surf. A Physicochem. Eng. Asp. **2008**, 323, 73–82.
(51) Koch, B. M.; Amirfazli, A.; Elliott, J. A. Wetting of rough surfaces by a low surface tension liquid. J. Phys. Chem. C **2014**, 118, 23777–23782.
(52) Koch, B. M.; Amirfazli, A.; Elliott, J. A. Modeling and measurement of contact angle hysteresis on textured high-contact-angle surfaces. J. Phys. Chem. C **2014**, 118, 18554–18563.
(53) Gibbs, J. W. On the equilibrium of heterogeneous substances. Am. J. Sci. **1878**, 16, 441–458.
(54) Ward, C.; Levart, E. Conditions for stability of bubble nuclei in solid surfaces contacting a liquid-gas solution. J. Appl. Phys. **1984**, 56, 491–500.
(55) Elliott, J. A.; Voitcu, O. On the thermodynamic stability of liquid capillary bridges. Can. J. Chem. Eng. **2007**, 85, 692–700.
(56) Eslami, F.; Elliott, J. A. Thermodynamic investigation of the barrier for heterogeneous nucleation on a fluid surface in comparison with a rigid surface. J. Phys. Chem. B **2011**, 115, 10646–10653.
(57) Zargarzadeh, L.; Elliott, J. A. Comparative surface thermodynamic analysis of new fluid phase formation between a sphere and a flat plate. Langmuir **2013**, 29, 3610–3627.
(58) Gong, W.; Zu, Y.; Chen, S.; Yan, Y. Wetting transition energy curves for a droplet on a square-post patterned surface. Sci. Bull. **2017**, 62, 136 – 142.
(59) Bico, J.; Thiele, U.; Quéré, D. Wetting of textured surfaces. Colloids Surf. A Physicochem. Eng. Asp. **2002**, 206, 41–46.
(60) Milne, A.; Amirfazli, A. The Cassie equation: How it is meant to be used. Adv. Colloid Interface Sci. **2012**, 170, 48–55.

Graphical TOC Entry